

Original Article

Ursolic acid inhibits the cholesterol biosynthesis and alleviates high fat diet-induced hypercholesterolemia *via* irreversible inhibition of HMGCS1 *in vivo*

Xiaoyao Ma^a, Yongping Bai^a, Kaixin Liu^a, Yiman Han^a, Jinling Zhang^a, Yuteng Liu^a, Xiaotao Hou^{b,*}, Erwei Hao^{b,*}, Yuanyuan Hou^{a,*}, Gang Bai^{a,*}

^a State Key Laboratory of Medicinal Chemical Biology, College of Pharmacy and Tianjin Key Laboratory of Molecular Drug Research, Nankai University, Tianjin, China

^b Guangxi Collaborative Innovation Center for Functional Ingredients Study of Agricultural Residues, Guangxi Key Laboratory of Efficacy Study on Chinese Materia Medica, Guangxi University of Chinese Medicine, Nanning, China



ARTICLE INFO

Keywords:

Ursolic acid
HMGCS1
Metabolite
Covalent binding
Cholesterol biosynthesis
Hypercholesterolemia

ABSTRACT

Background: In hypercholesterolemia, the concentrations of total cholesterol (TC) and low-density lipoprotein cholesterol (LDL-C) are enhanced in serum, which is strongly associated with an increased risk of developing atherosclerosis. Ursolic acid (UA), a pentacyclic terpenoid carboxylic acid, was found to alleviate hypercholesterolemia and hypercholesterolemia-induced cardiovascular disease. However, the specific targets and molecular mechanisms related to the effects of UA in reducing cholesterol have not been elucidated.

Purpose: In this study, we aimed to illustrate the target of UA in the treatment of hypercholesterolemia and to reveal its underlying molecular mechanism.

Methods: Nontargeted metabolomics was conducted to analyze the metabolites and related pathways that UA affected *in vivo*. The main lipid metabolism targets of UA were analyzed by target fishing and fluorescence colocalization in mouse liver. Molecular docking, in-gel fluorescence scan and thermal shift were assessed to further investigate the binding site of the UA metabolite with HMGCS1. C57BL/6 mice were fed a high-fat diet (HFD) for 12 weeks to induce hypercholesterolemia. Liver tissues were used to verify the cholesterol-lowering molecular mechanism of UA by targeted metabolomics, serum was used to detect biochemical indices, and the entire aorta was used to analyze the formation of atherosclerotic lesions.

Results: Our results showed that hydroxy-3-methylglutaryl coenzyme A synthetase 1 (HMGCS1) was the primary lipid metabolism target protein of UA. The UA metabolite epoxy-modified UA irreversibly bonds with the thiol of Cys-129 in HMGCS1, which inhibits the catalytic activity of HMGCS1 and reduces the generation of precursors in cholesterol biosynthesis *in vivo*. The contents of TC and LDL-C in serum and the formation of the atherosclerotic area in the entire aorta were markedly reduced with UA treatment in Diet-induced hypercholesterolemia mice.

Conclusion: UA inhibits the catalytic activity of HMGCS1, reduces the generation of downstream metabolites in the process of cholesterol biosynthesis and alleviates Diet-induced hypercholesterolemia *via* irreversible binding with HMGCS1 *in vivo*. It is the first time to clarify the irreversible inhibition mechanism of UA against HMGCS1. This paper provides an increased understanding of UA, particularly regarding the molecular mechanism of the cholesterol-lowering effect, and demonstrates the potential of UA as a novel therapeutic for the treatment of hypercholesterolemia.

Abbreviations: AcAc-CoA, acetoacetyl-CoA; Ac-CoA, acetyl-CoA; AEM-UA, alkynyl and epoxy-modified ursolic acid; ALT, alanine aminotransferase; AM-UA, alkynyl-modified ursolic acid; AST, aspartate aminotransferase; Ato, atorvastatin; CM-UA, carbonyl-modified ursolic acid; DMEM, Dulbecco's modified Eagle's medium; DTT, dithiothreitol; EM-UA, epoxy-modified ursolic acid; HDL-C, high-density lipoprotein cholesterol; HFD, high fat diet; HMG-CoA, hydroxy-3-methylglutaryl coenzyme A; HMGCR, hydroxy-3-methylglutaryl coenzyme A reductase; HMGCS1, hydroxy-3-methylglutaryl coenzyme A synthetase 1; IPP, isopentenyl pyrophosphate; KEGG, Kyoto Encyclopedia of Genes and Genomes; LDL-C, low-density lipoprotein cholesterol; MMs, Fe₃O₄ amino magnetic microspheres; Mod, model; ORO, oil red O; TBTA, Tris [(1-benzyl-1H-1,2,3-triazol-4-yl) methyl] amine; TC, total cholesterol; TCEP, tris (2-carboxyethyl) phosphine; TG, total triglyceride; UA, ursolic acid; WT, wild-type.

* Corresponding authors.

E-mail address: gangbai@nankai.edu.cn (G. Bai).

<https://doi.org/10.1016/j.phymed.2022.154233>

Received 4 January 2022; Received in revised form 21 May 2022; Accepted 31 May 2022

Available online 1 June 2022

0944-7113/© 2022 Elsevier GmbH. All rights reserved.

Introduction

Cholesterol is a necessary structural component of the plasma membrane, where it maintains a barrier between cells and the environment and regulates permeability and fluidity in cells. In mammals, it also serves as a substrate for the biosynthesis of bile acids, steroid hormones, and vitamin D. An insufficient supply of cholesterol produces detrimental effects on cell function, tissue development and whole-body physiology. The liver and small intestine are two crucial organs for cholesterol homeostasis in the body (Howles, 2016). However, excessive biosynthesis of cholesterol or hypercholesterolemia leads to enhanced concentrations of total cholesterol (TC) and low-density lipoprotein cholesterol (LDL-C) in serum. Accumulated evidence has demonstrated that an increased serum level of LDL-C is strongly associated with an increased risk of developing coronary artery disease and other atherosclerosis-related disorders (Lamb, 2020; Navarese et al., 2018).

Atherosclerosis is the pathological basis of most cardiovascular diseases, such as myocardial infarction, stroke, and peripheral artery disease, and is the leading cause of death and disability worldwide (Gianazza et al., 2021). The formation of atherosclerotic lesions is a chronic process characterized by excessive cholesterol deposition in the arterial intima (Yu et al., 2019). In the clinic, statins are commonly used to reduce LDL-C in treating hypercholesterolemia and atherosclerosis. It targets hepatocytes by binding with 3-hydroxy-3-methylglutaryl coenzyme A (HMG-CoA) reductase (HMGCR), which is a key regulator in the processes of cholesterol synthesis and inhibits the biosynthesis of cholesterol (Strilchuk et al., 2020).

There is growing interest in the health benefits associated with the consumption of phytochemicals from fruits, vegetables, and medicinal herbs (Del and Font, 2020). Ursolic acid (UA) is widely found in leaves, flowers and medicine herbs, such as rosemary and thyme, and has shown effects in preventing oxidative stress and inflammation, inhibiting the growth of cancer cells and alleviating liver injury (Naß and Efferth, 2021; Nguyen et al., 2021; Ma et al., 2021). Furthermore, the effects of UA on alleviating hypercholesterolemia and hypercholesterolemia-induced cardiovascular disease have also been reported. For example, UA exerted an antiatherogenic effect by decreasing the content of TC, modulating monocyte activity and reducing lesion formation in high-fat diet (HFD)-fed LDL receptor-deficient mice (Ullevig et al., 2011). In hypercholesterolemia hamsters, UA supplementation reduced the content of blood cholesterol by 15–16% (Hao et al., 2020). However, few studies have revealed the specific targets and molecular mechanisms of UA's reducing cholesterol effects in hypercholesterolemia and cardiovascular disease (Kim et al., 2019).

In this study, an alkynyl-modified UA (AM-UA) probe was prepared to trace and capture the target protein of UA from the liver *in vivo*. Subsequently, chemical proteome identification, chemical biological investigation and biochemical evaluation were undertaken to analyze the binding mode and binding site of UA. Targeted metabolomics was performed to verify the effects of UA in inhibiting cholesterol biosynthesis and alleviating hypercholesterolemia by targeting HMGCS1 *in vivo*.

Materials and methods

Reagents

UA (purity > 98.5%, determined by HPLC), 2-(7-azabenzotriazol-1-yl)-N, N, N, N-tetramethyluronium hexafluorophosphate (CAS:148,893–10–1), N, N-diisopropyl ethylamine (CAS: 7087–68–5) and *meta*-chloroperoxybenzoic acid (CAS: 937–14–4) were purchased from Aladdin (Beijing, China). Sodium 1-((3-((4-azidophenyl) dianyl) propanoyl) oxy)-2,5-dioxopyrrolidine-3-sulfonate was obtained from Bioworld (MN, USA). Fe₃O₄ amino magnetic microspheres (MMs) were purchased from Tianjin Baseline Chromtech Research Center (Tianjin,

China). Primary antibodies against HMG-CoA synthase 1 (HMGCS1) and secondary antibodies were obtained from Cell Signaling Technology (Beverly, MA, USA). Fluorescently labeled anti-rabbit IgG secondary antibodies were purchased from Abcam (Cambridge, UK). Chemiluminescent HRP substrates were obtained from Millipore Corporation (MA, USA). All the reagents used in cell culture were purchased from Gibco BRL Life Technologies (Grand Island, NY, USA).

Animal experiments and sample preparation

Male C57BL/6 mice (18–22 g) were purchased from the Experimental Animal Center of the National Institute for the Control of Pharmaceutical and Biological Products (Beijing, China, lot No. 0,006,407). The animals were housed in a suitable environment with *ad libitum* access to food and water. The mice were allowed to adjust to the housing situation for three days. The mice used in nontargeted metabolomics were randomly divided into two groups ($n = 6$), which were the control (Con) group and UA group (UA, 45 mg/kg daily). The mice used in targeted fishing and fluorescence analysis were randomly divided into two groups ($n = 6$): the UA group (UA, 45 mg/kg daily) and AM-UA group (alkynyl-modified ursolic acid, 45 mg/kg daily). The AM-UA probe (purity > 95%, determined by HPLC) was prepared as reported in our previous study (Ma et al., 2021) and received their treatments *via* gavage for 7 days. The animal experiments were approved by the Animal Ethics Committee, Guangxi University of Chinese Medicine (Nanning, China) and were performed in accordance with the guidelines of the national legislation of China. The use and care of mice for the study described herein was approved (2019-DW20190930–11).

Nontargeted metabolomics

The liver tissues of C57BL/6 mice were used for nontargeted metabolomics analysis. Nontargeted ultraperformance liquid chromatography (UPLC)-MS/MS analysis and metabolite identification were performed by Shanghai Applied Protein Technology Co., Ltd. (Shanghai, China), who provided technical support and in-depth discussions. The LC-MS analysis method and metabolite identification process was described in supplementary material. The metabolites with a VIP (variable importance for the project) value > 1 and $p < 0.05$ were selected as the significantly different metabolites. Then, the differentially expressed metabolites were enrichment-analyzed by the Kyoto Encyclopedia of Genes and Genomes (KEGG) to further explore the affected metabolic pathways.

Target fishing

Liver lysates from UA and AM-UA mice were prepared with pre-cooled RIPA lysis buffer (China COSCO, Beijing, China) and centrifuged at 4 °C for target fishing. The proteins were enriched by azide-modified functionalized MMs in a click reaction solution (1 mM CuSO₄, 1 mM TCEP and 0.1 mM TBTA in distilled water) at 37 °C for 2 h. After washing, the bound proteins were released with 200 μl DTT (100 mM) and analyzed by SDS-PAGE. The enriched proteins were identified by Huada Gene Co., Ltd. (Shenzhen, China).

Colocalization of the AM-UA probe with the target protein in the liver

The liver tissues of the UA- and AM-UA-treated mice were collected and fixed with 10% formalin. After fixation, the liver tissue sections were treated according to the instructions of the immunostain SP Kit (Tianjin Jiage, Tianjin, China) and incubated with a click reaction solution and 10 μM TMR azide fluorophore (Lumiprobe Corporation, Maryland, USA) at 37 °C for 30 min. After washing the Sections 3 times with PBST, the tissue sections were incubated with the HMGCS1 antibody (1:500) in 5% serum albumin at 4 °C overnight. The tissue sections were incubated with Alexa Fluor® 594-conjugated goat anti-rabbit

antibody (1:1000) for 30 min after washing 3 times with PBST. The fluorescence images were captured with a spectral-type LSM 700 confocal laser scanning microscope (Carl Zeiss, Oberkochen, Germany).

Molecular docking

The three-dimensional structures of the HMGCS1 protein (PDB: 2P8U) were obtained from the Protein Data Bank (<http://www.rcsb.org/pdb>). The structures of epoxy-modified UA (EM-UA) and HMGCS1 were constructed and minimized using SYBYL software (Chemical Computing Group, Inc.), then Schrödinger_2018 software (Schrödinger, Inc.) was applied for covalent docking, and the detailed protocol was as reported in our previous study (Ma et al., 2021). The binding mode and reaction site were analyzed by PyMOL software (Schrödinger, Inc.).

Fluorescence in-gel imaging

The alkynyl and epoxy-modified UA (AEM-UA, purity > 90%, determined by HPLC) probe, recombinant wild-type (WT) HMGCS1 and HMGCS1_S129G protein were prepared, and the synthesis process of AEM-UA and the expression and purification processes of recombinant proteins are shown in the supporting information. The protein contents of HMGCS1_WT and HMGCS1_S129G were incubated with 10 μ M AM-UA or 10 μ M AEM-UA for 4 h at 37 °C. The click reaction solution was added and incubated for 30 min at 37 °C. The solution was centrifuged and washed away by MeOH. The pelleted protein was dissolved in 0.2% SDS, and the supernatants were collected for SDS-PAGE. For in-gel fluorescence imaging, the gels were scanned on a PXi9 multifunction imager (Syngene, MD, USA). As a control test, the gels were stained with Coomassie blue staining for recombinant protein images.

Thermal shift assay

This experiment was performed as described in reference (Zhang et al., 2020) with some modifications. Briefly, the HMGCS1_WT and HMGCS1_S129G recombinant proteins were exposed to 10 μ M UA, 10 μ M carbonyl-modified UA (CM-UA, purity > 90%, determined by HPLC) or 10 μ M EM-UA (purity > 90%, determined by HPLC) for 4 h at 37 °C. Then, the protein was treated at different temperatures for 3 min and centrifuged at 4 °C and 1000 \times g for 10 min. The supernatant was collected for Western blot analysis.

Cell culture and biochemical indices analysis

The HepG2 cell line, derived from human hepatoma cells, was cultured in Dulbecco's modified Eagle's medium (DMEM) supplemented with 10% fetal bovine serum. The cells were obtained from the American Type Culture Collection (Manassas, VA, USA) and incubated at 37 °C in a 5% CO₂ atmosphere in a humidified incubator. OA- and PA-treated HepG2 cell models were established as *in vitro* models of lipid metabolism disorders as previously described (Dai et al., 2018). Briefly, cells were cultured in 96-well plates. When the cells reached approximately 60% confluence, they were treated with 1 mM free fatty acid (OA: PA= 2:1, molar ratio) with or without 10 μ M UA, 10 μ M CM-UA or 10 μ M EM-UA for 24 h. The lipid accumulation was measured by oil red O (ORO), and the contents of TC, LDL-C and high-density lipoprotein cholesterol (HDL-C) in cell lysates were measured using kits according to the manufacturers' instructions.

Diet-induced hypercholesterolemia in mice

C57BL/6 mice were randomly divided into six groups ($n = 6$), and the control group (Con) was fed a normal diet. The model group (Mod), atorvastatin group (Ato, 10 mg/kg daily), low-dose UA group (UA, 5 mg/kg daily), middle-dose UA group (UA, 15 mg/kg daily) and high-dose UA group (UA, 45 mg/kg daily) were fed a HFD and received

their treatments *via* gavage for 12 weeks. The HFD contains 40% energy as fat, 1.25% cholesterol and 0.5% sodium cholate (Jiangsu Xietong Pharmaceutical Bioengineering Ltd, Jiangsu, China). The sera of mice were used for biochemical index analysis by a Pointcare M3 biochemistry analyzer (MNCHIP, Tianjin, China). The livers of mice were collected and fixed with 10% formalin. After fixation and sectioning, liver tissue slices were used for ORO staining and hematoxylin and eosin (H&E) staining. The aortas were longitudinally incised and fixed with 10% formalin and then stained with ORO solution for detection of atherosclerotic lesions. Images were captured with a digital single-lens reflex camera, and the percentage of ORO-positive area was calculated by dividing ORO-positive areas by the area of the entire aorta, which was measured by ImageJ software.

Targeted metabolomics

The liver tissues of Con group, HFD group and high-dose UA Group C57BL/6 mice were used for targeted metabolomics analysis. Targeted ultraperformance liquid chromatography (UPLC)-MS/MS analysis and metabolite identification were performed by Qingdao Sci-tech innovation Testing Co., Ltd. (Qingdao, China), who provided technical support and in-depth discussions. The LC-MS analysis method and metabolite identification process was described in supplementary material. All MS files (mzXML format) were processed using MultiQuan (Sciex™) for peak detection, alignment and normalization. Based on the in-house spectral library, compounds with SNRs greater than 3 were extracted to generate an identification list, and the peak area was normalized based on the weighting of the tissue.

Statistical analysis

The results are expressed as the mean values \pm standard deviation (SD). Differences between two groups were analyzed by *t*-tests, and differences between multiple groups were analyzed by analysis of variance followed by Bonferroni's test. $p < 0.05$ was considered statistically significant. All data were processed using GraphPad Prism statistical software, version 5.01.

In addition, the statistical analysis of metabolomics was described in supplementary material.

Results

Metabolomics revealed that UA affects lipid metabolism

Nontargeted metabolomics was conducted to analyze the metabolites and related pathways that UA affected *in vivo*. After screening, 52 significantly different metabolites are shown in the volcano figure (Fig. 1A), and the cluster analysis is shown in the heatmap (Fig. 1B). Then, the significantly different metabolites were analyzed for their functions and the degree of enrichment according to the KEGG metabolic pathway, and the significance of their enrichment in each pathway was calculated using Fisher's exact test. As shown in Fig. 1C, the glycerolipid metabolism pathway was the most significantly affected by UA. There were four significantly different metabolites, D-glycerate, glycerol 3-phosphate, D-glucose 1-phosphate and 2-phosphoglycerate, in the glycerolipid metabolism pathway. This result suggested that UA influenced the lipid metabolism of the liver *in vivo*.

HMGCS1 was identified as a potential target of UA

To analyze the main lipid metabolism targets of UA, AM-UA was used to capture the potential targets and fluorescent analysis in the livers of C57BL/6 mice (Fig. 2A). Fluorescence in-gel imaging showed that AM-UA was available for target analysis *in vivo* and was mainly distributed in the liver compared to other tissues (Fig. 2B). The captured proteins from liver lysates were analyzed *via* SDS-PAGE with Coomassie brilliant

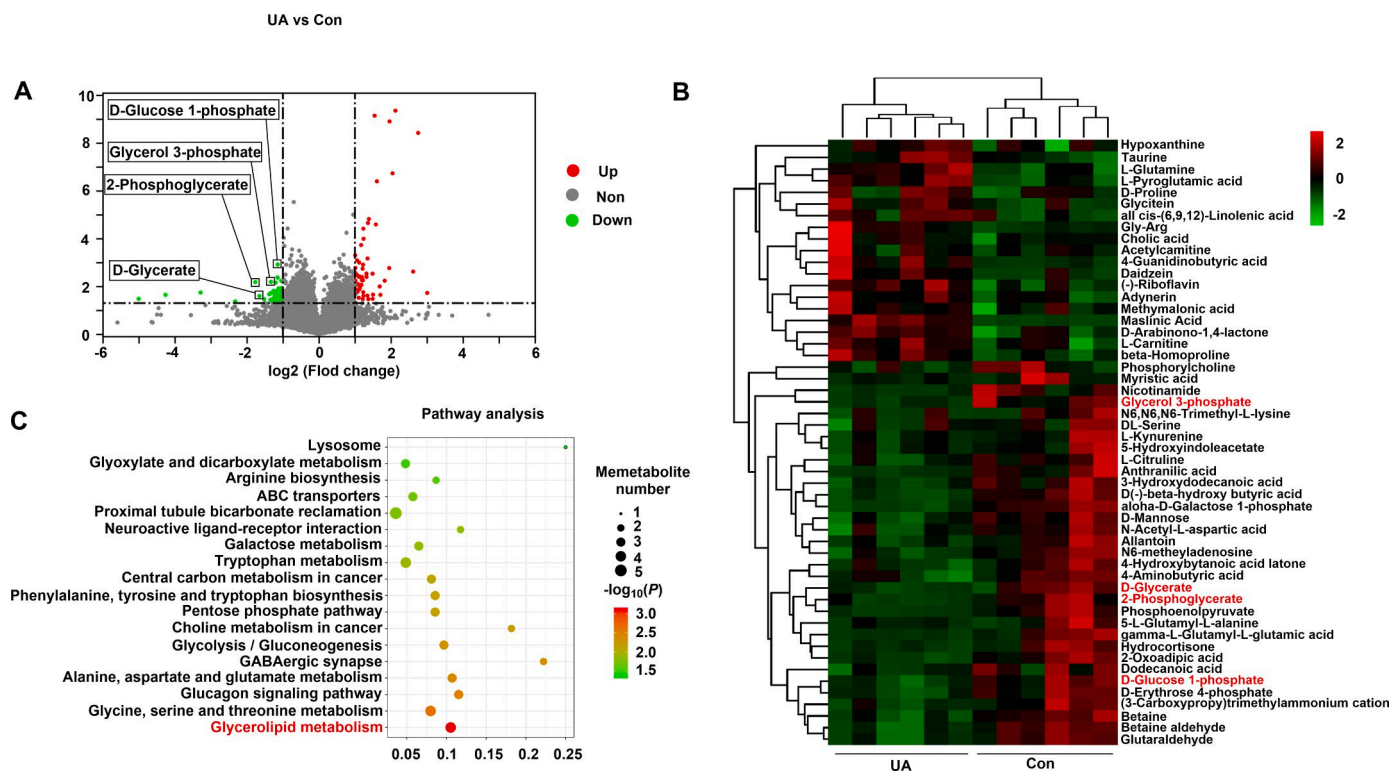


Fig. 1. Nontargeted metabolomics analysis of the liver in C57BL/6 mice. (A) Screening of significantly different metabolites affected by UA *in vivo*. (B) Cluster analysis and (C) metabolic pathway enrichment of the significantly different metabolites.

blue staining. Compared to the UA group (Lane 2, negative control group), the AM-UA group (Lane 3) enriched more proteins, which were potential targets of UA (Fig. 2C). Q-Exactive HF X was used to identify the captured proteins and analyze the potential targets of UA according to the mass scores of the captured proteins in the AM-UA group and UA group. The differentially expressed proteins were subjected to functional analysis by KEGG analysis. The HMGCS1 protein was identified as a lipid metabolism-associated target of UA (Yao et al., 2020) (Fig. 2D). To further verify the result, Western blots were used to verify the most likely target of HMGCS1 enrichment. As expected, the approximately 57-kDa HMGCS1 protein band was enriched in the AM-UA group compared to that in the UA group (Fig. 2E), which is consistent with the target screening result, suggesting that AM-UA might label HMGCS1 *in vivo*.

To verify the results of the target fishing strategy, the colocalization of HMGCS1 and AM-UA was investigated in liver sections. As shown in Fig. 2F, pseudogreen fluorescence of the AM-UA probe was observed only in the liver sections of the AM-UA group. The distribution of HMGCS1, which was stained pseudored with a Cy3 antibody, was observed in hepatocytes. After amplification, fluorescence imaging showed that AM-UA appeared to partially colocalize with the HMGCS1 protein in hepatocytes (pseudoyellow). The above results indicated that HMGCS1 was the primary target protein of UA *in vivo*.

Epoxy metabolite of UA covalently bound with CYS-129 of HMGCS1

A previous study illustrated that UA could be metabolized into epoxy-modified UA (EM-UA), which has the potential to react with nucleophilic groups in target proteins *in vivo* (Hu et al., 2018). To further analyze the binding site of the UA metabolite with HMGCS1, Schrödinger_2018 software was used to provide additional insights into the interaction of EM-UA and HMGCS1 (PDB: 2P8U). The docking settings imitated the potential covalent binding poses of EM-UA with nucleophilic groups of HMGCS1. In all cases, the top-scoring pose of EM-UA

was displayed as 3D maps (Fig. 3A). The structure of HMGCS1 is constituted by thiolase fold, extension and HMGCS-specific folds (Shafiqat et al., 2010). The epoxy group of EM-UA covalently bound with Cys-129 in a thiolase fold. Moreover, the hydroxy group of EM-UA, which was generated in the process of epoxy group reaction with Cys-129, established hydrogen bonds with His-264 and Asn-343 in thiolase fold. In the sequence comparison of HMGCS1_HUMAN and HMGCS1_MOUSE, the thiolase fold was conserved, and the residues that interacted with EM-UA were the same in both humans and mice (Fig. 3B). To verify the molecular docking results, AM-UA and AEM-UA were used for fluorescence in-gel imaging (Fig. 3C). Coomassie brilliant blue analysis showed that the four samples contained the same amounts of protein. The in-gel fluorescence scan showed a fluorescence band in the AEM-UA reacted with HMGCS1_WT. However, there were no fluorescence bands in the AM-UA reacted with HMGCS1_WT or HMGCS1_C129G, which suggested that the epoxy group is necessary for the covalent binding of EM-UA with HMGCS1. The AEM-UA reacted with HMGCS1_C129G and showed no fluorescence band in the in-gel fluorescence scan, which verified that the epoxy group only reacted with the thiol group of Cys-129 in HMGCS1 (Fig. 3D).

To further evaluate the specific effects of EM-UA, UA and CM-UA, an EM-UA analog that replaces the epoxy group with a carbonyl group was used with EM-UA for comparative studies by thermal shift analysis. As shown in Fig. 3E, EM-UA significantly increased the thermal stability of the HMGCS1 recombinant protein, and UA and CM-UA had no effect. Moreover, EM-UA, UA and CM-UA did not affect the thermal stability of the HMGCS1_C129G recombinant protein (Fig. 3F). The above results demonstrated that EM-UA covalently binds with the thiol group of Cys-129 in HMGCS1.

Epoxy metabolites of UA inhibited the biosynthesis of cholesterol by binding HMGCS1

HMGCS1 catalyzes the condensation of acetoacetyl-CoA (AcAc-CoA)

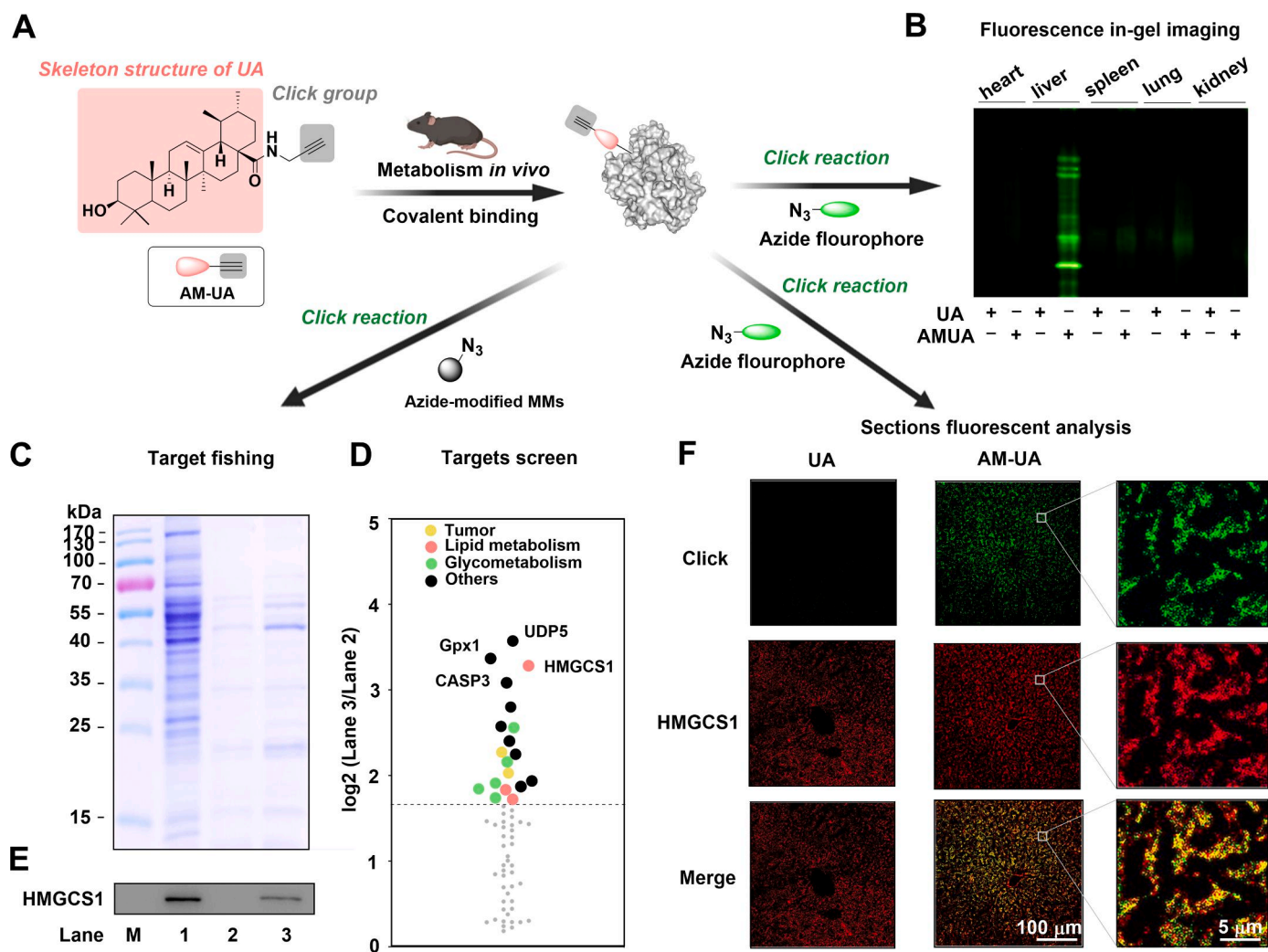


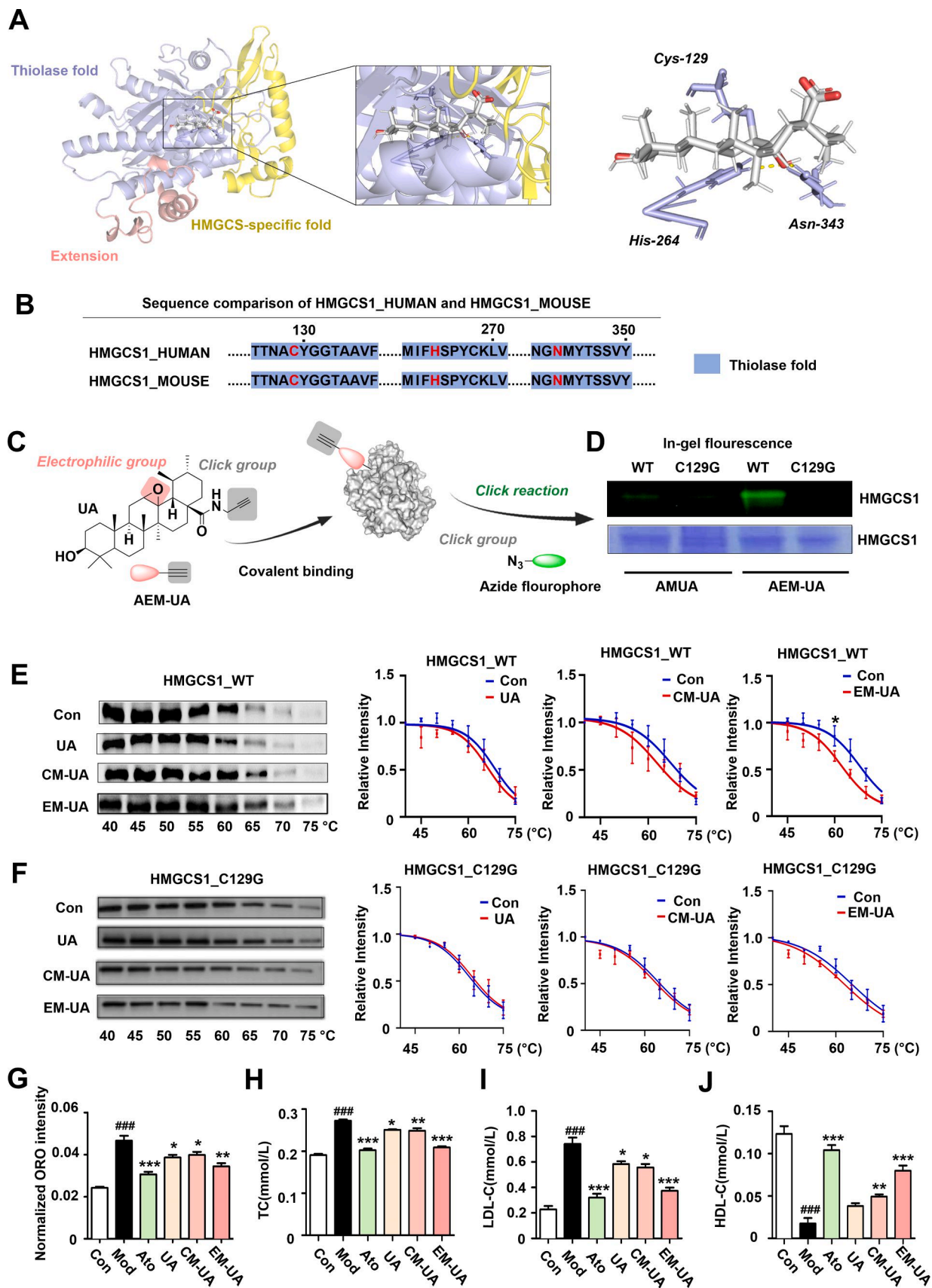
Fig. 2. HMGCS1 was identified as the lipid metabolism target of UA *in vivo*. (A) The processes of fluorescence analysis and target fishing *in vivo*. (B) Fluorescence in-gel imaging was performed to analyze the distribution in the heart, liver, spleen, lung and kidney. (C) Coomassie brilliant blue staining was used to detect the proteins enriched by AM-UA from the livers of mice. (D) Scatter diagram of differential protein profiling captured by AM-UA. (E) Western blot analysis was used to detect HMGCS1 among the enriched proteins (Lane 1, the total liver lysate of mice; Lane 2, the protein captured by azide-modified MMs; Lane 3, the protein captured by UA-modified MMs). (F) The colocalization of HMGCS1 (pseudored) and the AM-UA probe (pseudogreen) in liver sections.

and acetyl-CoA (Ac-CoA) to form HMG-CoA and CoA, which is necessary for *de novo* synthesis of cholesterol (Vögeli et al., 2018). In the structure of HMGCS1, nucleophilic Cys-129 attacks the carbonyl carbon of Ac-CoA for the subsequent catalysis process (Shafiqat et al., 2010). The UA metabolite EM-UA covalently binds with the catalytic nucleophile Cys-129, which may affect the catalytic process of HMGCS1. Hence, we evaluated the ability of EM-UA to lower oleic acid- and palmitic acid-induced lipid accumulation in HepG2 cells. UA, CM-UA or EM-UA inhibited lipid accumulation and reduced the contents of TC and LDL-C (Fig. 3G-I). The content of HDL-C was decreased by oleic acid and palmitic acid and increased following the addition of UA, CM-UA or EM-UA (Fig. 3J). However, the effect of EM-UA by covalent binding was much stronger than that of UA and CM-UA at the same dose. This result suggests that EM-UA inhibited the biosynthesis of cholesterol by binding HMGCS1 and that the epoxy group produced by metabolism plays an important role in the inhibitory effect on HMGCS1.

UA inhibited precursor generation for cholesterol biosynthesis *in vivo*

The process of cholesterol biosynthesis consists of three phases: the synthesis of isopentenyl pyrophosphate (IPP) by Ac-CoA, IPP inverts to squalene and squalene generates cholesterol (Fig. 4A). HMGCS1 is in the

phase of Ac-CoA inverts to IPP. Because nontargeted metabolomics did not detect metabolites in the process of cholesterol biosynthesis, targeted metabolomics was performed to detect the contents of 5 key metabolites in this pathway. Mice were fed a HFD for 12 weeks to induce hypercholesterolemia, and we found that UA affected the expression of metabolites in the liver. The change trends of 5 key metabolites are shown in a heatmap (Fig. 4B). Then, the relative sensitivity of key metabolites compared to the Con group was determined for further analysis. As shown in Fig. 4C and D, the substrates HMGCS1, Ac-CoA and AcAc-CoA were markedly enhanced in the HFD group and HFD treatment with UA group. However, HMG-CoA, the product of HMGCS1, was significantly increased in the HFD group and significantly decreased after treatment with UA (Fig. 4E). The downstream metabolites mevalonate and IPP were also significantly increased in the HFD group and significantly decreased after treatment with UA (Fig. 4F and G). The targeted metabolomics results suggested that UA inhibited the catalytic activity of HMGCS1 and reduced the generation of cholesterol precursors *in vivo*.



(caption on next page)

Fig. 3. Binding site analysis of UA with HMGCS1. (A) Molecular modeling of HMGCS1 and UA. PyMOL software was used to construct 3D maps of the covalent interaction between HMGCS1 (PDB: 2P8U) and UA. UA and Cys-129 are displayed as sticks and colored according to atom type, with carbon atoms in gray and oxygen atoms in red. (B) Sequence homology alignment of HMGCS1 between humans and mice. (C) The process of AEM-UA labeling with HMGCS1 and in-gel fluorescence analysis. (D) Coomassie blue staining and in-gel fluorescence scanning were used to analyze the HMGCS1_WT and HMGCS1_C129G proteins labeled with AM-UA or AEM-UA. Thermal transformation analysis was used to evaluate the thermal stability of (E) HMGCS1_WT and (F) HMGCS1_C129G recombinant proteins with or without UA, CM-UA or EM-UA. The residual recombinant protein contents of HMGCS1_WT and HMGCS1_S40G were detected by Western blot and are presented as the mean \pm SD according to the normalized intensity ($n = 3$, $*p < 0.05$ compared to the Con group). HepG2 cells were stimulated with oleic acid and palmitic acid for 24 h with or without treatment with 10 μ M UA, 10 μ M CM-UA or 10 μ M EM-UA. (G) The lipid accumulation was measured by ORO. The contents of (H)TC, (I) LDL-C and (J) HDL-C were measured by kits ($n = 6$, $###p < 0.001$ compared to the Con group; $*p < 0.05$, $**p < 0.01$, $***p < 0.001$ compared to the Mod group).

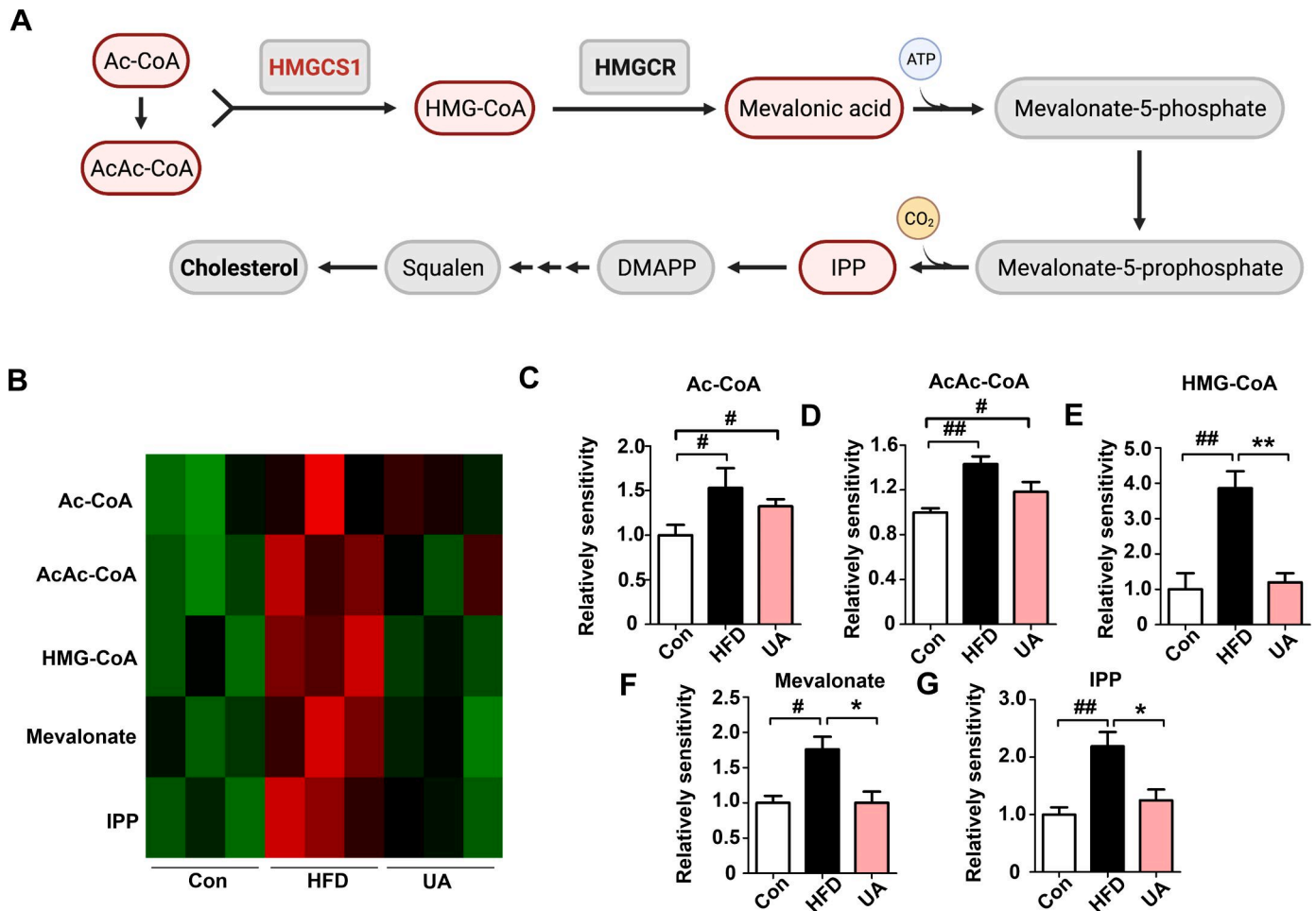


Fig. 4. Targeted metabolomics analysis of UA affected the catalytic activity of HMGCS1. (A) The process of cholesterol biosynthesis from Ac-CoA and AcAc-CoA. (B) Heatmap analysis of 5 key metabolites in cholesterol biosynthesis. The metabolite relative sensitivity analysis of (C) Ac-CoA, (D) AcAc-CoA, (E) HMG-CoA, (F) mevalonate and (G) IPP are presented as the mean \pm SD ($n = 3$, $#p < 0.05$, $##p < 0.01$ compared to the Con group; $*p < 0.05$, $**p < 0.01$ compared to the HFD group).

UA inhibited cholesterol biosynthesis and alleviated diet-induced hypercholesterolemia by binding with HMGCS1 in vivo

In Diet-induced hypercholesterolemic mice, we first evaluated the biochemical indices in serum, which were detected by an automatic biochemical analyzer. UA inhibited the generation of precursors in cholesterol biosynthesis via inhibition of HMGCS1, which was further confirmed by the effects on TC, LDL-C, HDL-C and total triglyceride (TG) levels in serum. The TC, LDL-C and TG contents increased and the HDL-C content decreased in the mice fed a HFD. However, the contents of TC, LDL-C and TG were markedly reduced, and the content of HDL-C was markedly enhanced by treatment with UA in a dose-dependent manner. Ato exerted a similar effect on lipid metabolism regulation as UA by inhibiting HMGCR, which is the downstream reductase of HMGCS1 in

cholesterol biosynthesis (Fig. 5A–D). Diet-induced hepatocytes underwent necrosis, which caused an increase in ALT and AST content and a decrease in total protein and albumin content in serum. The middle-dose UA group, high-dose UA group and Ato group showed a significant reduction in hepatocyte necrosis and the contents of ALT and AST and an increase in the contents of total protein and albumin (Fig. 5E–H). Meanwhile, glucose was enhanced in the HFD group and decreased by treatment with UA or Ato (Fig. 5I). The contents of urea, homocysteine and globulin (Fig. 5J–L) were unchanged in serum.

Lipid accumulation in the liver was analyzed by ORO staining, and as shown in Fig. 5M, Ato or UA decreased the Diet-induced accumulation of hepatic lipids. H&E staining of liver samples from HFD-fed animals showed that the structure of the liver lobule was deformed, the arrangement of hepatocyte cords was disordered, and the hepatocytes

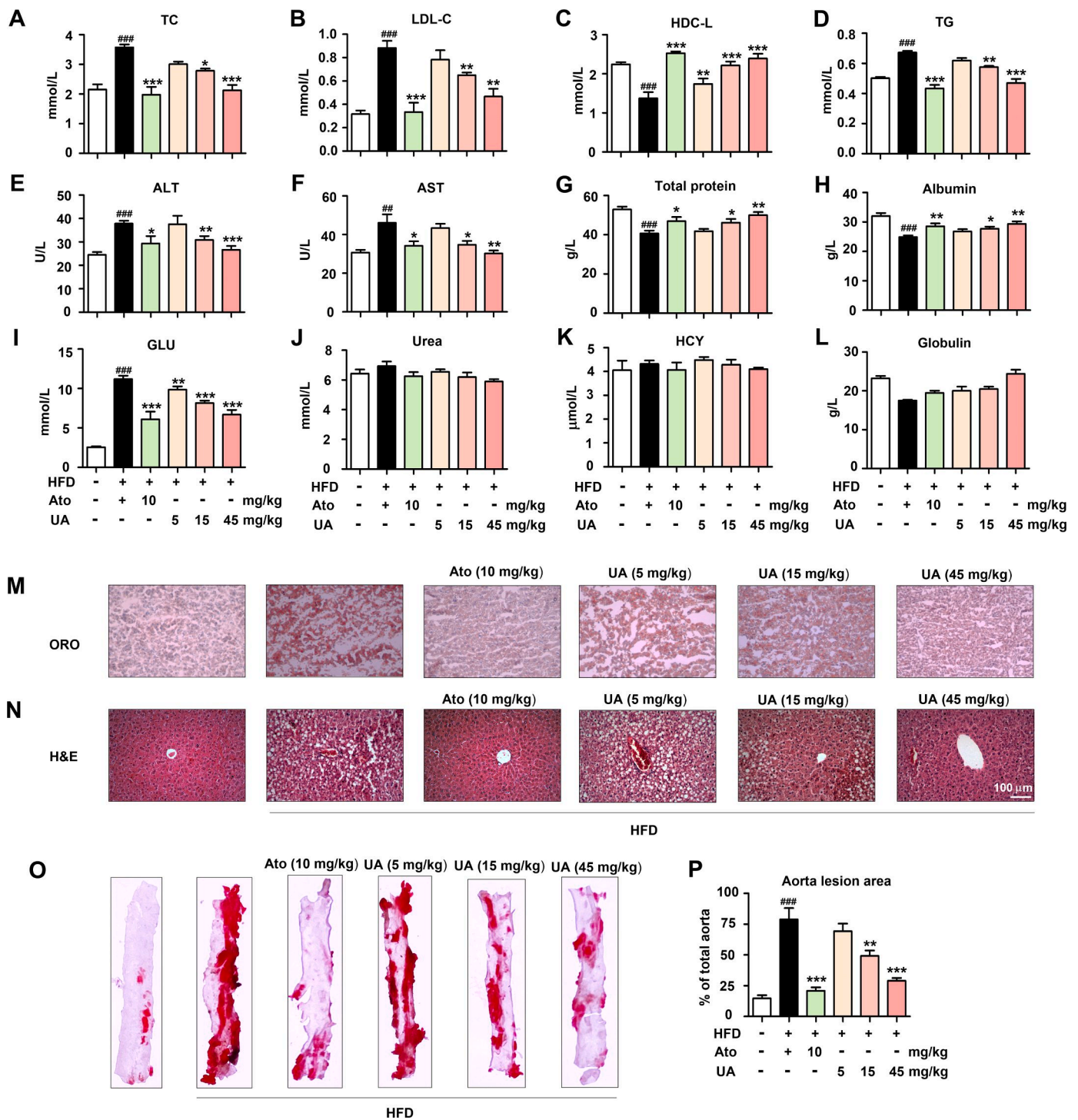


Fig. 5. UA alleviates Diet-induced hypercholesterolemia and arteriosclerosis by inhibiting HMGCS1 *in vivo*. Diet-induced hypercholesterolemic mice were treated with Ato or UA, and the contents of (A) TC, (B) LDL-C, (C) HDL-C, (D) TG, (E) ALT, (F) AST, (G) total protein, (H) albumin, (I) Glu, (J) urea, (K) HCY and (L) globulin in serum were analyzed by a Pointcare M3 biochemistry analyzer ($n = 6$). (M) Lipid accumulation in the liver was observed by ORO, and (N) histopathological changes in the liver were observed by H&E staining. (O) Atherosclerotic lesions in the entire aorta were observed by ORO and (P) measured by ImageJ software ($n = 6$, $##p < 0.01$, $###p < 0.001$ compared to the Con group; $*p < 0.05$, $**p < 0.01$, $***p < 0.001$ compared to the HFD group).

underwent edema and necrosis. Treatment with Ato or UA reduced the degree of pathological liver changes and showed normal histology (Fig. 5N). Feeding a HFD promoted the formation of atherosclerotic lesions, whereas supplementation with UA and Ato significantly suppressed the formation of the atherosclerotic area in the entire aorta (Fig. 5O–P). The above results suggested that UA reduced the generation of cholesterol and LDL-C to relieve hypercholesterolemia and

arteriosclerosis by inhibiting HMGCS1.

Discussion

Cholesterol biosynthesis is a complex biochemical process that mainly proceeds in the liver and involves more than 30 different reactions utilizing over 15 enzymes (Luo et al., 2020). The process begins

with the generation of HMG-CoA by HMGCS1, and the membrane-bound enzyme HMGCR converts HMG-CoA to mevalonate, which is a precursor for cholesterol synthesis. This part of the reaction is often considered to be the principal flux-governing step in the process of cholesterol biosynthesis, and statin drugs target HMGCR to inhibit cholesterol biosynthesis in the treatment of hypercholesterolemia and atherosclerosis (Wilding et al., 2000; Mizioro, 2011). Therefore, HMGCS1 is also a potential drug target for regulating serum cholesterol levels. Molecular probe-based target analysis suggested that UA was mainly distributed in liver tissue and bound with HMGCS1 in the liver. Combined with the metabolomics results, UA affected the principal flux-governing step of cholesterol biosynthesis and decreased the generation of HMG-CoA and mevalonate by inhibiting the catalytic activity of HMGCS1. The biosynthesis of cholesterol was affected by UA in the liver, which caused the contents to decrease TC and LDL-C in serum. The benefits were considered the potential mechanism by which UA alleviates hypercholesterolemia and atherosclerosis.

HMGCS1 catalyzes one molecule of Ac-CoA and one molecule of AcAc-CoA to form HMG-CoA, which is the first committed step in the de novo synthesis of cholesterol (Vögeli et al., 2018). The catalysis reaction is a three-step ping-pong reaction, including a conserved Cys-His-Glu-catalytic triad and an acyl-enzyme intermediate (Misra and Mizioro, 1996). First, His264 acts as a catalytic base or H-bond donor for nucleophilic Cys129, which attacks the carbonyl carbon of Ac-CoA and forms acetylated Cys129 (Campobasso et al., 2004). Our study demonstrates that the epoxide metabolite of UA acts as a ligand that targets and reacts with Cys129 in the thiolase fold of HMGCS1, which prevents the formation of acetylated Cys129 in HMGCS1. Acetylated Cys129 is necessary for subsequent reactions, and its methyl group is deprotonated by the general base Glu95 to form a carbanion, which attacks AcAc-CoA and forms HMG-CoA (Chun et al., 2000). Because EM-UA irreversibly binds with Cys129, the reaction of Ac-CoA and AcAc-CoA is blocked in HMGCS1, which leads to decreases in the generation of HMG-CoA and cholesterol *in vivo*.

Hypercholesterolemia causes cholesterol accumulation in the liver, which provokes the production of reactive oxygen species and redox imbalance (Förstermann, 2008; Bin-Jumah, 2018). Oxidative stress induces the activation of caspase3, hepatocyte apoptosis and liver damage during hypercholesterolemia (Bayatmakoo et al., 2017). Meanwhile, the caspase inhibitor Z-VAD-FMK diminished cholesterol-induced cell apoptosis (Li et al., 2020). Our previous study illustrated that UA increased the content of superoxide dismutase and irreversibly inhibited caspase3 to reduce hepatocellular apoptosis and alleviate alcohol-induced liver injury *in vivo* (Ma et al., 2021). In the present study, the high-dose UA group exerted a similar inhibitory effect on cholesterol biosynthesis as the Ato group. However, the ALT and AST contents decreased, and the total protein content increased more markedly in the high-dose UA treatment group than in the Ato group, which suggested that UA also acted as an antioxidant and inhibited caspase3 to alleviate cholesterol-induced hepatocyte apoptosis and necrosis in hypercholesterolemia.

Currently, there is a concern surrounding the use of natural compounds or products to prevent chronic diseases. The brine shrimp test showed that UA has low toxicity with an LC₅₀ of 0.95 mg/ml, and daily oral gavage administration of UA showed no toxicity effect at 1000 mg/kg in rats for 90 consecutive days (Somova et al., 2003; Geerlofs et al., 2020). In clinical pharmacokinetic and safety study, the healthy adult volunteers, who took UA at single oral doses up to 1000 mg orally, exerted no serious adverse event (Hirsh et al., 2014). In this paper, we found that the survival rates of mice were not affected by the dose of 45 mg/kg UA. Moreover, the epoxy electrophilic group of UA metabolite irreversibly bonds with Cys129 in HMGCS1, which plays a more lasting and effective role in inhibiting the catalytic activation of HMGCS1 and the process of cholesterol biosynthesis than traditional competitive inhibitors. Based on the above studies, daily oral of UA is safe and can lead to a reduced risk of hypercholesterolemia.

In conclusion, our findings suggest that UA reduces the generation of HMG-CoA and downstream metabolites in the process of cholesterol biosynthesis and alleviates Diet-induced hypercholesterolemia *via* the irreversible inhibition of HMGCS1 *in vivo*, which was the first time to elucidate the cholesterol-lowering target of UA and clarified its irreversible inhibition mechanism against HMGCS1. These results provide an increased understanding of UA, particularly regarding the molecular mechanism of the cholesterol-lowering effect, and demonstrate the potential of UA as a novel therapeutic for the treatment of hypercholesterolemia.

Declaration of Competing Interest

The authors declare no conflicts of interest.

Acknowledgments

This research was supported by Guangxi Collaborative Innovation Center for Functional Ingredients Study of Agricultural Residues(CICAR 2019-Z3)and Guangxi Key Laboratory of Efficacy Study on Chinese Materia Medica (19-245-1).

Supplementary materials

Supplementary material associated with this article can be found, in the online version, at doi:10.1016/j.phymed.2022.154233.

References

- Bayatmakoo, R., Rashtchizadeh, N., Yaghmaei, P., Farhoudi, M., Karimi, P., 2017. Atorvastatin inhibits cholesterol-induced caspase-3 cleavage through down-regulation of p38 and up-regulation of Bcl-2 in the rat carotid artery. *Cardiovasc. J. Afr.* 28, 298–303.
- Bin-Jumah, M.N., 2018. Monolluma quadrangula protects against oxidative stress and modulates LDL receptor and fatty acid synthase gene expression in hypercholesterolemic rats. *Oxid. Med. Cell. Longev.* 2018, 3914384.
- Campobasso, N., Patel, M., Wilding, I.E., Kallender, H., Rosenberg, M., Gwynn, M.N., 2004. *Staphylococcus aureus* 3-hydroxy-3-methylglutaryl-CoA synthase: crystal structure and mechanism. *J. Biol. Chem.* 279, 44883–44888.
- Chun, K.Y., Vinarov, D.A., Zajicek, J., Mizioro, H.M., 2000. 3-Hydroxy-3-methylglutaryl-CoA synthase. A role for glutamate 95 in general acid/base catalysis of C-C bond formation. *J. Biol. Chem.* 275, 17946–17953.
- Dai, J., Liang, K., Zhao, S., Jia, W., Liu, Y., Wu, H., Lv, J., Cao, C., Chen, T., Zhuang, S., Hou, X., Zhou, S., Zhang, X., Chen, X.W., Huang, Y., Xiao, R.P., Wang, Y.L., Luo, T., Xiao, J., Wang, C., 2018. Chemoproteomics reveals baicalin activates hepatic CPT1 to ameliorate diet-induced obesity and hepatic steatosis. *Proc. Natl. Acad. Sci. U. S. A.* 115, E5896–E5905.
- Del, Río-Celestino, M., Font, R., 2020. The health benefits of fruits and vegetables. *Foods* 9, 369.
- Förstermann, U., 2008. Oxidative stress in vascular disease: causes, defense mechanisms and potential therapies. *Nat. Clin. Pract. Cardiovasc. Med.* 5, 338–349.
- Geerlofs, L., He, Z., Xiao, S., Xiao, Z.C., 2020. Repeated dose (90 days) oral toxicity study of ursolic acid in Han-Wistar rats. *Toxicol. Rep.* 7, 610–623.
- Gianazza, E., Brioschi, M., Martinez Fernandez, A., Casalnuovo, F., Altomare, A., Aldini, G., Banfi, C., 2021. Lipid peroxidation in atherosclerotic cardiovascular diseases. *Antioxid. Redox Signal.* 34, 49–98.
- Hao, W., Kwek, E., He, Z., Zhu, H., Liu, J., Zhao, Y., Ma, K.Y., He, W.S., Chen, Z.Y., 2020. Ursolic acid alleviates hypercholesterolemia and modulates the gut microbiota in hamsters. *Food Funct.* 11, 6091–6103.
- Hirsh, S., Huber, L., Zhang, P., Stein, R., Joyal, S., 2014. A single ascending dose, initial clinical pharmacokinetic and safety study of ursolic acid in healthy adult volunteers (1044.6). *FASEB J.* 28, 1044–1046.
- Howles, P.N., 2016. Cholesterol absorption and metabolism. *Methods Mol. Biol.* 1438, 177–197.
- Hu, X.Y., Shen, Y.B., Yang, S.N., Lei, W., Cheng, L., Hou, Y.Y., Bai, G., 2018. Metabolite identification of ursolic acid in mouse plasma and urine after oral administration by ultra-high performance liquid chromatography/quadrupole time-of-flight mass spectrometry. *RSC Adv.* 8, 6532–6539.
- Kim, G.H., Kan, S.Y., Kang, H., Lee, S., Ko, H.M., Kim, J.H., Lim, J.H., 2019. Ursolic acid suppresses cholesterol biosynthesis and exerts anti-cancer effects in hepatocellular carcinoma cells. *Int. J. Mol. Sci.* 26, 4767.
- Lamb, Y.N., 2020. Rosuvastatin/ezetimibe: a review in hypercholesterolemia. *Am. J. Cardiovasc. Drugs* 20, 381–392.
- Li, K., Deng, Y., Deng, G., Chen, P., Wang, Y., Wu, H., Ji, Z., Yao, Z., Zhang, X., Yu, B., Zhang, K., 2020. High cholesterol induces apoptosis and autophagy through the ROS-activated AKT/FOXO1 pathway in tendon-derived stem cells. *Stem Cell Res. Ther.* 11, 131.

- Luo, J., Yang, H., Song, B.L., 2020. Mechanisms and regulation of cholesterol homeostasis. *Nat. Rev. Mol. Cell. Biol.* 21, 225–245.
- Ma, X.Y., Zhang, M., Fang, G., Cheng, C.J., Wang, M.K., Han, Y.M., Hou, X.T., Hao, E.W., Hou, Y.Y., Bai, G., 2021. Ursolic acid reduces hepatocellular apoptosis and alleviates alcohol-induced liver injury via irreversible inhibition of CASP3 *in vivo*. *Acta Pharmacol. Sin.* 42, 1101–1110.
- Misra, I., Mizioro, H.M., 1996. Evidence for the interaction of avian 3-hydroxy-3-methylglutaryl-CoA synthase histidine 264 with acetoacetyl-CoA. *Biochemistry* 35, 9610–9616.
- Miziorko, H.M., 2011. Enzymes of the mevalonate pathway of isoprenoid biosynthesis. *Arch. Biochem. Biophys.* 505, 131–143.
- Naß, J., Efferth, T., 2021. Ursolic acid ameliorates stress and reactive oxygen species in *C. elegans* knockout mutants by the dopamine Dop1 and Dop3 receptors. *Phytomedicine* 81, 153439.
- Navarese, E.P., Robinson, J.G., Kowalewski, M., Kolodziejczak, M., Andreotti, F., Bliden, K., Tantry, U., Kubica, J., Raggi, P., Gurbel, P.A., 2018. Association between baseline LDL-C level and total and cardiovascular mortality after LDL-C lowering: a systematic review and meta-analysis. *JAMA* 319, 1566–1579.
- Nguyen, H.N., Ullevig, S.L., Short, J.D., Wang, L., Ahn, Y.J., Asmis, R., 2021. Ursolic acid and related analogues: triterpenoids with broad health benefits. *Antioxidants* 10, 1161.
- Shafiqat, N., Turnbull, A., Zschocke, J., Oppermann, U., Yue, W.W., 2010. Crystal structures of human HMG-CoA synthase isoforms provide insights into inherited ketogenesis disorders and inhibitor design. *J. Mol. Biol.* 398, 497–506.
- Somova, L.O., Nadar, A., Rammanan, P., Shode, F.O., 2003. Cardiovascular, antihyperlipidemic and antioxidant effects of oleanolic and ursolic acids in experimental hypertension. *Phytomedicine* 10, 115–121.
- Strilchuk, L., Tocci, G., Fogacci, F., Cicero, A.F.G., 2020. An overview of rosuvastatin/ezetimibe association for the treatment of hypercholesterolemia and mixed dyslipidemia. *Expert Opin. Pharmacother.* 21, 531–539.
- Ullevig, S.L., Zhao, Q., Zamora, D., Asmis, R., 2011. Ursolic acid protects diabetic mice against monocyte dysfunction and accelerated atherosclerosis. *Atherosclerosis* 219, 409–416.
- Vögeli, B., Engilberge, S., Girard, E., Riobé, F., Maury, O., Erb, T.J., Shima, S., Wagner, T., 2018. Archaeal acetoacetyl-CoA thiolase/HMG-CoA synthase complex channels the intermediate via a fused CoA-binding site. *Proc. Natl. Acad. Sci. U. S. A.* 115, 3380–3385.
- Wilding, E.I., Brown, J.R., Bryant, A.P., Chalker, A.F., Holmes, D.J., Inghram, K.A., Iordanescu, S., So, C.Y., Rosenberg, M., Gwynn, M.N., 2000. Identification, evolution, and essentiality of the mevalonate pathway for isopentenyl diphosphate biosynthesis in gram-positive cocci. *J. Bacteriol.* 182, 4319–4327.
- Yao, W., Jiao, Y., Zhou, Y., Luo, X., 2020. KLF13 suppresses the proliferation and growth of colorectal cancer cells through transcriptionally inhibiting HMGCS1-mediated cholesterol biosynthesis. *Cell Biosci.* 10, 76.
- Yu, X.H., Zhang, D.W., Zheng, X.L., Tang, C.K., 2019. Cholesterol transport system: an integrated cholesterol transport model involved in atherosclerosis. *Prog. Lipid Res.* 73, 65–91.
- Zhang, W.Y., Gao, J., Cheng, C.J., Zhang, M., Liu, W.J., Ma, X.Y., Lei, W., Hao, E.W., Hou, X.T., Hou, Y., Bai, G., 2020. Cinnamaldehyde enhances antimelanoma activity through covalently binding ENO1 and exhibits a promoting effect with dacarbazine. *Cancers (Basel)* 12, 311.